"Thermally stable and flame retardant polymer nanocomposites"
V.Mittal (Editor) (c) Cambridge University Press, 2011

# Chapter 4

# Poly(ethylene terephthalate) nanocomposites using nanoclays modified with thermally stable surfactants

EVANGELOS MANIAS,[a] MATTHEW J. HEIDECKER,[a,c] HIROYOSHI NAKAJIMA,[a,d] MARIUS C. COSTACHE,[b,e] AND CHARLES A. WILKIE[b]

[a] *Polymer Nanostructures Lab–Center for the Study of Polymer Systems (CSPS) and The Pennsylvania State University*
[b] *Marquette University*
[c] *Emerson Climate Technologies*
[d] *Sumitomo Chemical Co. Ltd.*
[e] *Rutgers University*

## 4.1 Introduction

The term "nanocomposite" is widely used to describe a very broad range of materials, where one of the phases has a submicrometer dimension [1–4].[1] In the case of polymer-based nanocomposites, this typically involves the incorporation of "nano" fillers with one (platelets), two (fibers, tubes), or all three dimensions at the submicrometer scale. However, strictly speaking, simply using nanometer-scaled fillers is not sufficient for obtaining genuine/true nanocomposites [5]: these fillers must also be well dispersed down to individual particles *and* give rise to intrinsically new properties, which are not present in the respective macroscopic composites or the pure components. In this chapter, we shall use a broader definition, encompassing also "nanofilled polymer composites" [5], where – even without complete dispersion or in the absence of any new/novel functionalities – there exist substantial concurrent enhancements of multiple properties (for example, mechanical, thermal, thermomechanical, barrier, and flammability). Further, we shall limit our discussion to one example, focusing on poly(ethylene terephthalate) (PET) with mica-type layered aluminosilicates.

The fact that nanometer-thin layered inorganics can be dispersed in macromolecular matrices is ubiquitous in nature, and it has also long been established in the laboratory; for example, synthetic polymers were shown to disperse appropriately-modified clay minerals before the 1960s [6, 7]. However, the field of polymer/layered-silicate

[1] This work is an overview of projects supported through various funding agencies and industrial sources. In particular, financial support by Bayer MaterialScience and by the Sumitomo Chemical Company is acknowledged. Work at Marquette University was supported by the Habermann Fund, MJH was supported through an ES&F ARL fellowship, HN by Sumitomo Chemical (Japan), and EM by the National Science Foundation (NSF DMR-0602877) and the "Virginia and Philip Walker" endowment. The authors would like to thank Dr. Cheng Fang Ou for providing us with his data, plotted in Figure 4.7d.

nanocomposites has gained substantial new momentum from the perspective of high-performance composite materials in the last decade. This renewed research interest was catalyzed by three main breakthroughs: first, pioneering work by the Toyota research group, who reported the preparation of a high-performance polyamide-6/layered-silicate nanocomposite [8, 9]; subsequently, the discovery by Giannelis and co-workers that it is possible to melt-process such composites [10], eliminating the need for organic solvents or new polymerization schemes; and finally, the work at NIST where it was first unveiled how nanosized clay fillers can impart a general flame-retardant character to polymers [11]. Since then, the field has been actively pursued, mostly because of the opportunities for concurrent enhancements in mechanical, thermal, barrier, and flammability properties [12–16] afforded by the addition of small amounts of clay (cf. nanofilled polymer composites).

Typically, marked property enhancements in nanocomposites originate from the nanometer-scale dispersion of highly anisotropic inorganic fillers in the polymer matrix and, thus, appropriate organic modification of the inherently hydrophilic clay fillers is a crucial step in the design and preparation of high-performing materials [16–19]. Among the modifiers used for nanoclays, quaternary ammonium surfactants are the most common because – besides their low cost and commercial availability – they can render these fillers miscible with a broad range of polymer matrices [18]. However, in the case of PET, alkylammonium surfactants are inadequate because, although they possess the proper favorable thermodynamics of mixing, they do not have the required thermal stability, neither for in situ PET polymerization nor for melt-processing of PET nanocomposites.

At this point, we should also mention that this chapter is not intended to provide an extensive review of the polymer nanocomposites field – the reader interested in such reviews can refer to a number of related books [1–4], numerous compilations of relevant symposia and conference proceedings, or recent review articles [12–15, 20, 21]. This chapter is rather an attempt to establish design principles toward the formation of PET nanocomposites with layered silicates bearing thermally stable surfactants, as well as linking these design principles to the relevant underlying fundamentals.

## 4.2 Melt-processable poly(ethylene terephthalate)/organosilicate nanocomposites

### *4.2.1 Challenges of PET nanocomposite formation*

Because both melt-processing and polymerization of PET necessitate high temperatures (250–300 °C), it becomes obvious at the outset that any organically modified layered silicates that are intended as reinforcing fillers for PET should employ surfactants with appropriately high thermal stability. The typical alkylammoniums, for example, decompose below these temperatures. Two examples of higher-temperature surfactants that have been employed as modifiers for layered silicates in PET nanocomposites are pyridinium and phosphonium; specifically, cetylpyridinium, via solution dispersion [22], and dodecyltriphenylphosphonium, via in situ polymerization [23]. In these two cases, both the

pyridinium and phosphonium surfactants possess sufficiently high decomposition temperatures to survive, for example, the second stage of the polymerization reaction (typically [23], 2 h at 280 °C). At the same time, the single alkane of the surfactant, dodecyl or cetyl, satisfies the thermodynamic requirements for mixing [17], because in these two examples it is only required that the organo-montmorillonites be miscible with small-molecule organics: for the solution mixing, the organofiller should disperse in a solvent (3:1 phenol: chloroform) in which PET is dissolved [22], or for the in situ polycondensation, the organofiller should disperse in the ethylene glycol, which is later reacted with dimethyl terephthalate [23].

For melt-processing of PET nanocomposites, the requirements for the organically modified layered silicates are even more stringent, because, in addition to high temperatures, melt-processing requires prolonged exposure to oxidizing environments. Thus, successful preparation of good melt-processed PET nanocomposites presents great challenges. Successful nanocomposite preparation, in this case, implies thermodynamically favored nanometer-scale dispersion of the layered silicates, with no marked decomposition of the organofillers or of the PET matrix, processed under typical extrusion and injection-molding conditions for PET. Specifically, all the following requirements should be satisfied by the organic modification of the layered silicates:

1. *The organosilicate must possess sufficiently favorable thermodynamics of mixing with PET*: that is, the surfactant should promote mixing in PET nanocomposites with thermally stable organoclays within the typical residence time in an extruder (ca. 1–3 min). This requirement translates [16, 17] into the existence of one or two long-alkyl chains, for example, hexadecyl [24, 25] or octadecyl, or two hexadecyls [26]. Shorter alkyls are also possible, although they lead to poorer dispersion [24]. The incorporation of additional polar or polarizable groups into the surfactant, such as hydroxyls or phenyls, substantially *reduces* the thermodynamic free energy of mixing with PET.
2. *The surfactant must have high enough thermal stability to survive the typical melt-processing conditions of PET*: namely, it should have a decomposition temperature above 300 °C. This requirement is not met, for example, by alkylammoniums that have a decomposition temperature of about 250 °C. However, this requirement can be satisfied by large classes of surfactants, such as phosphonium-, imidazolium-, and pyridinium-based molecules.
3. *The organosilicates should be deprived of water as much as possible*, because PET is sensitive to water and will decompose under melt-processing conditions in the presence of water traces. This requirement is very important but, surprisingly, rather neglected. Most organically modified silicates contain measurable amounts of water that cannot be removed by drying: for example, alkylammonium and alkylphosphonium montmorillonites contain 5–8 wt% water that is hydrogen-bonded to the silicon oxide cleavage planes, which cannot be removed even after drying indefinitely under vacuum slightly above 100 °C; this water is often termed “structural water” and its removal requires drying temperatures of 350–450 °C under vacuum [27].

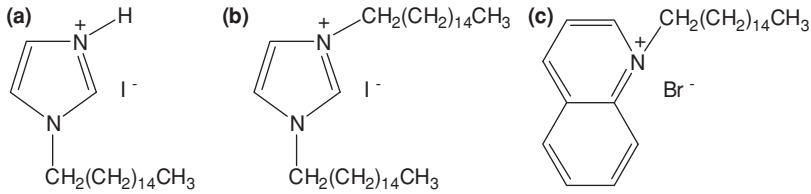


Figure 4.1 Chemical structures of (a) hexadecyl-imidazolium [26], (b) dihexadecyl-imidazolium [26], and (c) hexadecyl-quinolinium [25].

### 4.2.2 High–thermal stability surfactants for PET nanocomposites

In this chapter, we focus on *melt-processed* PET/nanoclay nanocomposites, where the nanoclay is alkylimidazolium montmorillonite or alkylquinolinium montmorillonite. The chemical structures of these thermally stable alkyl cations are shown in Figure 4.1, and both the surfactants and the respective organically modified clays can be synthesized easily (see Section 4.5). These imidazolium and quinolinium surfactants satisfy all three requirements for application to melt-processable PET nanocomposites, as enumerated in Section 4.2.1. Specifically,

1. These surfactants satisfy the requirement for *favorable thermodynamics of mixing with PET*, by virtue of their one or two long alkyl chains [17]. For example, Vaia and Giannelis [17, 18] employed a balance of entropic and enthalpic contributions – akin to those for polymer blends – to quantify the free energy change for dispersion of organically modified nanoclays in a polymer. In a first approximation, this mode defines the enthalpy change per interlayer-gallery area upon mixing by[2]

$$\Delta H \propto \varphi_{\mathrm{p}}\varphi_{\mathrm{a}}(\gamma_{\mathrm{ap}} + \gamma_{\mathrm{sp}} - \gamma_{\mathrm{sa}}) \tag{4.1}$$

where the subscripts correspond to the various system components (layered silicate s, alkyl surfactant a, and polymer p); $\varphi_{\mathrm{p}}$, $\varphi_{\mathrm{a}}$ are the interlayer volume fractions of polymer and surfactant; and $\gamma_{ij}$ are the interfacial surface tensions describing the interactions between $i$ and $j$ components. Further, the gain in enthalpy upon filler dispersion, viz., the "competitive adsorption" interactions ($\Delta\gamma$, the difference of interfacial surface tensions in the parentheses in eq. (4.1)) can be calculated in a mean-field manner through pairwise interfacial surface tensions,

$$\gamma_{ij} = \gamma_{ij}^{\mathrm{LW}} + \gamma_{ij}^{\mathrm{AB}}, \text{ with } \begin{cases} \gamma_{ij}^{\mathrm{LW}} \cong \left(\sqrt{\gamma_i^{\mathrm{LW}}} - \sqrt{\gamma_j^{\mathrm{LW}}}\right)^2 \\ \gamma_{ij}^{\mathrm{AB}} \cong 2\left(\sqrt{\gamma_i^{+}} - \sqrt{\gamma_j^{+}}\right)\left(\sqrt{\gamma_i^{-}} - \sqrt{\gamma_j^{-}}\right) \end{cases} \tag{4.2}$$

[2] In eq. (4.1) a number of proportionality constants [such as the monomeric volume fractions of polymer and surfactant in the interlayer, the surface area per surfactant, and the gallery height ($h = d_{001} - 0.97$ nm) of the intercalated structure] are omitted. Readers interested in the detailed calculation of $\Delta H$ are referred to the theoretical papers [17, 18].

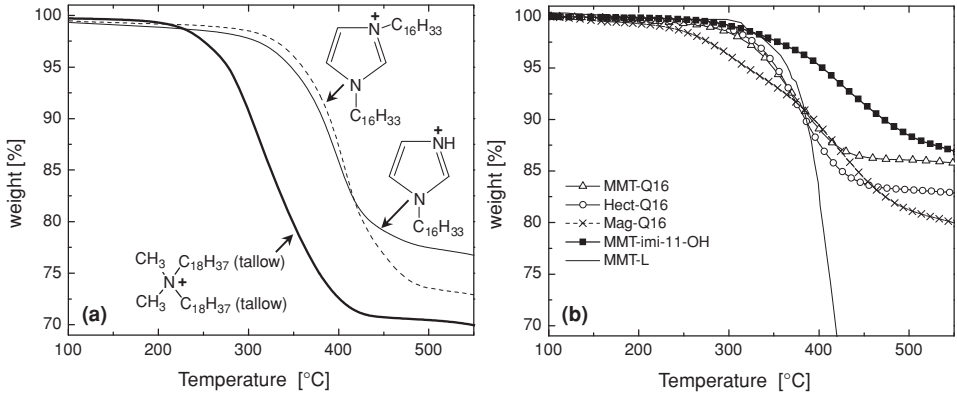


Figure 4.2 Thermal stability of organically modified clays: (a) TGA curves for hexadecylimidazolium montmorillonite and dihexadecylimidazolium montmorillonite compared with di(tallow-alkyl)ammonium montmorillonite (heating rate 10 °C/min under nitrogen [26]). (b) TGA curves of MMT cationically exchanged with 1-(11-hydroxy-undecyl)-2,3-dimethyl-3H-imidazol-1-ium) [Imi-11OH] and three hexadecylquinolinium modified clays (montmorillonite [MMT-Q16], hectorite [Hect-Q16], and magadiite [Mag-Q16], all run at a heating rate of 20 °C/min under nitrogen [25]).

where the $\gamma_{ij}$ interfacial surface tension are calculated based on the surface tension contributions from each component ($\gamma_i$ and $\gamma_j$) following standard geometric combination rules and the van Oss–Chaudhury–Good formalization [28]; the LW, AB superscripts denote the nature of the interactions (apolar, Lifschitz–van der Waals LW; polar, Lewis-acid/Lewis-base AB), with $\gamma_i^+$ representing the electron-acceptor character of $i$, and $\gamma_i^-$ representing the electron-donor character (thus, $\gamma_i^{AB} \cong 2\sqrt{\gamma_i^+ \gamma_i^-}$). The $\gamma$ component values ($\gamma^{LW}, \gamma^+, \gamma^-$) are well established for all materials considered here, with (66, 0.7, 36 mJ/m$^2$) for montmorillonite [18, 29]; (28, 0, 0 mJ/m$^2$) for long-chain ($C_{16}$–$C_{18}$) alkyls [29]; and (43.5, 0.01, 6.8 mJ/m$^2$) for PET [30]. Substituting these values into eq. (4.2) gives excess enthalpy upon mixing PET with alkyl-modified montmorillonite that is approximately $\Delta\gamma \approx -8.5$ mJ/m$^2$, indicating a rather high favorable energy of mixing (comparable to that of polyamide-6,6 in alkyl montmorillonite $\Delta\gamma \approx -9.9$ mJ/m$^2$, and larger than that of polystyrene in alkyl montmorillonite $\Delta\gamma \approx -5.5$ mJ/m$^2$).

Despite the approximations and the simplicity of this model, this line of thought clearly indicates that PET would show very good dispersion in hexadecyl montmorillonite (better than the intercalated PS structure, and comparable with the mostly exfoliated polyamide); this fact has been confirmed experimentally [24] and is also seen for our systems (see Section 4.3).

2. These surfactants also possess *sufficiently high thermal stability to survive the melt-processing conditions of any PET grade*. As shown in Figure 4.2, the decomposition temperatures of nanoclays organically modified with alkylimidazolium are above 300–320 °C, with a peak decomposition temperature around 400 °C, whereas the typical

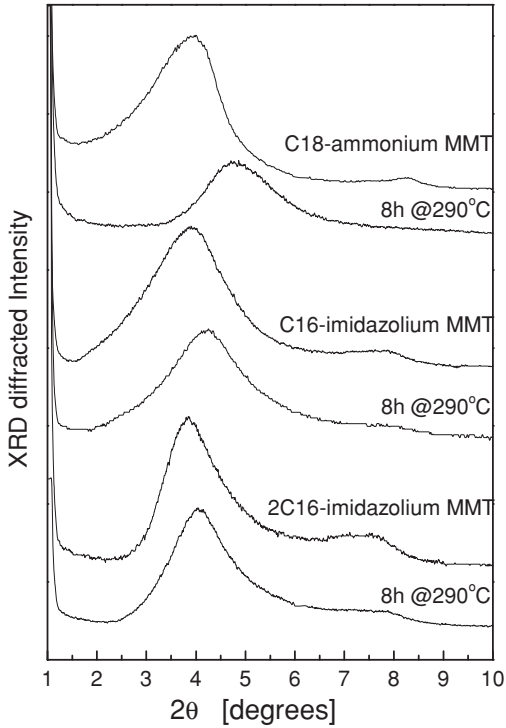


Figure 4.3 Thermal stability of organically modified MMT as reflected in XRD patterns (top) before and (bottom) after heat treatment at 290 °C for 8 h in vacuo. From top to bottom, three organo-MMT systems are shown: MMT modified by octadecylammonium (top two patterns), hexadecylimidazolium (middle two patterns), and dihexylimidazolium (bottom two patterns). Figure reproduced with permission from Wang *et al*. [26], © 2003 Wiley.

extrusion temperatures for PET are 240–280 °C and the typical injection molding temperature for PET is 260–300 °C (depending on application). In comparison, the same nanoclays modified by alkylammonium have a decomposition temperature of about 250 °C (Figure 4.2), which effectively renders them inapplicable under PET melt-processing conditions. Alternatively, instead of TGA, the thermal stability of the same organoclays can be quantified by X-ray diffraction after isothermal annealing at 290 °C in vacuo (Figure 4.3), which further demonstrates that alkylimidazolium montmorillonites can survive these temperatures, whereas alkylammonium montmorillonites cannot, as was indicated by the TGA behavior (Figure 4.2). In addition, substitution of methyl groups for the two hydrogens in the 2 and 3 positions of the imidazole ring offers even higher thermal stability [24, 31, 32] than the surfactants shown in Figures 4.1 (a, b), but may have lower efficacy for eliminating water from within the nanoclay interlayer galleries and for attaching two pending hydrophobic tails (cf. requirements 3 and 1). Along the same lines, even when PET/nanoclay composites are produced through an in situ

polymerization scheme (typically polycondensation of ethylene glycol with dimethyl terephthalate in the presence of the nanofiller), the organic modification of the fillers still needs to survive a few hours at 250–280 °C in the second stage of the reaction. Although here the temperatures are slightly lower than for melt-processing, the alkylammonium surfactants still cannot meet the thermal stability requirements, whereas alkylimidazolium [33], -pyridinium [22], or -phosphonium [23] surfactants, or even acids [34], do.

3. Finally, a third important requirement is that *surfactant-treated fillers intended for PET nanocomposites should be deprived of water* as much as possible. This is particularly important in melt-processed PET nanocomposites, because water can be liberated from the nanofillers during extrusion and dramatically decompose the PET (hydrolysis). Removal of water becomes even more critical for clay nanofillers, because the pristine silicates are very hydrophilic and contain substantial amounts of structural water [6]. This structural water cannot be removed by standard practices of drying [27], but needs to be driven out of the interlayer gallery spaces by organic modification. This requirement implies that the surfactant should create a very hydrophobic environment in the interlayer gallery that would drive any structural water out and would prevent subsequent rehydration. Alternatively, water can be removed efficiently from alkylammonium or alkylphosphonium clays, if during the last stages of the organoclay preparation, washing is done with distilled organic solvents that form organoclay suspensions; however, these organoclays would readily rehydrate under ambient storage conditions. In contrast, alkylimidazolium surfactants do create a sufficiently hydrophobic environment in the interlayer gallery, which limits, or completely prevents, subsequent rehydration. Along these lines, dialkyl surfactants are more effective than monoalkyl equivalents – by virtue of their stronger hydrophobic character – and imidazole is probably more effective than quinoline or dimethyl-substituted imidazole – both of which tend to arrange flat on the silicate cleavage plane, when intercalated or surface end-tethered.

In summary, when surfactants are selected for nanofillers intended for PET nanocomposites, there are important requirements that should be met, substantially limiting the range of appropriate surfactants. As a first approach, alkylammoniums should be avoided, whereas alkylimidazoliums should be preferred. This last class of surfactants are applicable to high-performance nanocomposites beyond PET; for example, they were successfully used in polystyrene and polyamide matrices [32], epoxies [35], and ABS polymers [36, 37], as well as for fillers other than clays, such as polyhedral oligomeric silsesquioxane (POSS) [38] and carbon nanotubes [39].

### 4.3 Characterization and performance of poly(ethylene terephthalate)/clay nanocomposites

As examples of the utilization of thermally stable imidazolium-based surfactants with montmorillonite (MMT), allowing high-temperature melt-blending of PET nanocomposites,

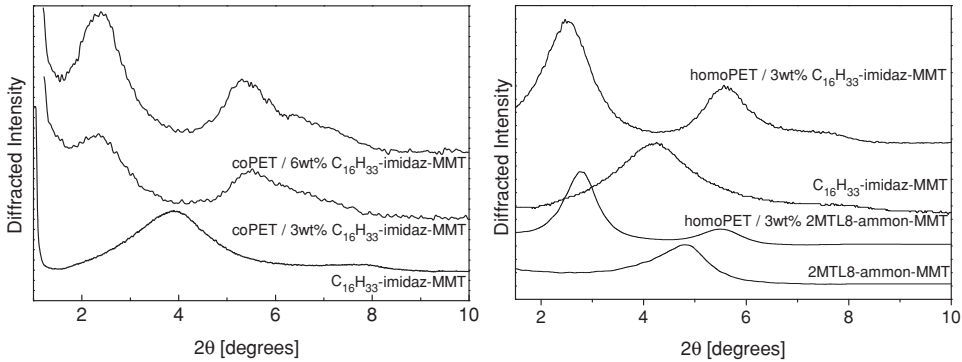


Figure 4.4 X-ray diffraction of alkylimidazolium montmorillonite (MMT) and the respective melt-processed nanocomposites with PET: (Left) XRD curves for hexadecylimidazolium MMT and its nanocomposites with copolymer-PET. (Right) XRD curves of MMT organically modified with dimethyl-tallow-2-ethylhexyl quaternary ammonium [2MTL8-ammon-MMT] and with hexadecylimidazolium [$C_{16}H_{33}$-imidaz-MMT] and their respective nanocomposites with homopolymer-PET.

we compare two categories of poly(ethylene terephthalate): PET homopolymer [*homo-PET*, with high molecular weight ($M_w$ = 61 kg/mol) and high intrinsic viscosity (IV = 0.95 dL/g), Voridian-12822] and PET copolymer (*co-PET*, poly(ethylene terephthalate-*co*-isophthalate), $M_w$ = 33 kg/mol, IV = 0.64 dL/g, Kosa-1101). The focus is on elucidating the effect of the organo-MMT nature on the composite morphology of melt-processed PET nanocomposites and, further, compare the mechanical, thermal and fire properties between selected melt-processed PET nanocomposites.

### 4.3.1 Filler dispersion and composite morphology

The composite morphology was studied by Bragg-reflection powder X-ray diffraction (XRD, Figure 4.4) and by transmission electron microscopy (TEM, Figure 4.5). As a first approach, XRD can be used to assess the nanocomposite structure, because the $d_{001}$ basal reflection is indicative of filler–filler separation (*intercalated* composite morphologies). In Figure 4.4 we compare the XRD patterns of organically modified montmorillonites before and after melt-processing them with PET (extrusion followed by injection molding). For both copolymer (blow-molding grade) PET and homopolymer (crystallizable) PET, a definitive shift of the $d_{001}$ basal reflection to higher $d$-spacings (lower $2\theta$ diffraction angles) denotes the insertion of PET within the interlayer gallery of the hexadecylimidazolium montmorillonites; at the same time, the disappearance of the diffraction peak that corresponds to the organoclay (at $2\theta \sim 4^\circ$ or $d_{001} \sim 2.2$ nm) denotes that all the organoclay was swollen or dispersed by PET. In addition, similar XRD studies of alkylammonium-modified MMT (Figure 4.4) also show gallery expansion of the organoclay upon melt-blending with PET, despite very considerable thermal degradation of the alkyl quaternary ammonium and some decomposition of the PET. However, the XRD can

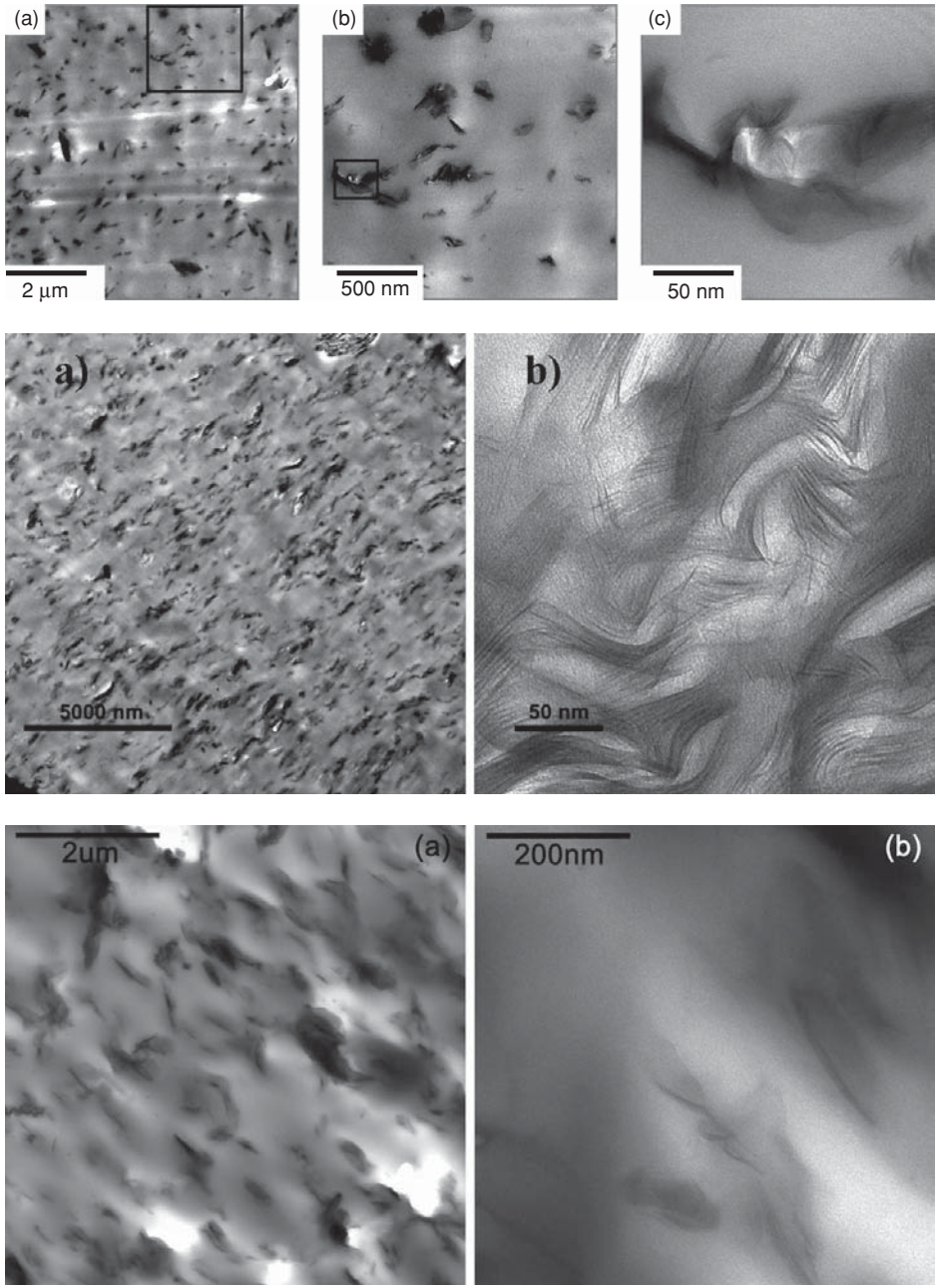


Figure 4.5 Bright-field TEM of the hierarchical composite structure (at the μm and nm length scales) of melt-processed PET/organo-MMT nanocomposites. (top) Melt-processed copolymer-PET/3 wt% $C_{16}H_{33}$–imidazolium MMT; boxes indicate the region of the subsequent higher-magnification image [44]. (middle) Melt-processed homopolymer-PET/3 wt% $C_{16}H_{33}$–imidazolium MMT [44]. (bottom) Melt-processed homopolymer-PET/3 wt% $C_{16}H_{33}$–quinolinium MMT [25]. © 2010, 2006 Wiley, reproduced with permission.

only detect the distance between periodically stacked layers; *disordered* (bunched together but not parallel stacked) or *exfoliated* layers are not detected by powder XRD. Although detailed quantitative analysis of XRD data in the low-2$\theta$ range, based on carefully prepared samples and the use of model reference samples, can yield substantially more information about the nanocomposite structure [40], powder XRD is still insufficient to capture and characterize the complete nanocomposite structure.[3] Thus, the XRD results need to be complemented by scattering techniques [41, 42], or by direct imaging of the composite structure, such as through transmission electron microscopy (TEM), to properly describe the diversity of nanostructures present in the nanocomposite [43].

In Figure 4.5, we show representative bright-field TEM pictures highlighting the hierarchical structures across length scales – from μm (agglomerates, tactoids) to nm (single montmorillonite layers). The structure of nanocomposites for co-PET and homo-PET with alkylimidazolium- and alkylquinolinium-modified MMT is shown. In all cases, organoclay dispersion in the polymer matrix is generally good, with no extended MMT agglomerates present. At the μm scale, filler tactoids are well dispersed throughout the polymer, most often separated by clay stacks of 2 to 4 layers and – to a lesser extent – single (exfoliated) MMT layers. At the nm scale, the higher-magnification images illustrate both intercalated and disordered structure, as individual layers of the fillers are expanded by the polymer penetration, often maintaining some of their parallel registry. It is tempting to note that as viscosity increases, so does the apparent tactoid dispersion, with homo-PET here showing better dispersion than co-PET; however, it must be mentioned that homo-PET is also more thermodynamically favored to disperse these organoclays than co-PET, given the aliphatic comonomer in the latter. These morphologies are in excellent agreement with the XRD observations, that is, shifted, broad, low-intensity $d_{001}$ diffraction peaks and raised-intensity background (Figure 4.4). These composite structures are also consistent with a well-dispersed clay nanofiller composite morphology, showing the typical coexistence of intercalated, disordered, and exfoliated organoclay layers.[4]

### 4.3.2 Mechanical properties

The mechanical properties of the bulk PET and its nanocomposites were measured by tensile testing on injection-molded microtensile dogbones (ASTM-D638, Type IV) and by dynamic mechanical analysis (DMA) on injection-molded bars.

Tables 4.1 and 4.2 show the tensile properties of homo-PET and co-PET and their montmorillonite nanocomposites. For all nanocomposites, both with thermally stable imidazolium surfactants and with alkylammoniums, the tensile moduli increased compared to the respective unfilled PET (by 15% to 30%, for 3 wt% inorganic content) because of the montmorillonite addition. The magnitude of this modulus improvement is as expected

[3] In general, for the type of particles used here, that is, natural clays with medium (ca. 1 μm) lateral-size platelets, even with favorable thermodynamics for polymer nanocomposite formation, the composite structure is almost always characterized by the coexistence of exfoliated, intercalated, and disordered layers. Thus, a silent XRD may hide a large number of disordered tactoids, whereas an XRD with an intercalated peak does not reveal the extent of exfoliation.

[4] See note 3.

Table 4.1 *Tensile properties of homopolymer PET and its nanocomposites with alkylimidazolium (hexadecylimidazolium, $im_{16}$) and alkylammonium (dimethyl tallow 2ethylhexylammonium, 2MTL8, $am_{18.8}$) montmorillonite*

| MMT content $\varphi_{mmt}$ (wt%) | Tensile modulus $E$ (MPa) | Yield strength $\sigma_{yield}$ (MPa) | Elongation at break $\varepsilon_{max}$ (%) |
|---|---|---|---|
| 0 | 1550 ± 50 | 55 ± 2 | 230 ± 15 |
| 3 $im_{16}$ | 1830 ± 25 | 59 ± 1 | 202 ± 35 |
| 0 | 1550 ± 50 | 55 ± 2 | 230 ± 15 |
| 3 $am_{18,8}$ | 1860 ± 25 | 60 ± 1 | 115 ± 15 |
| 6 $am_{18,8}$ | 2080 ± 75 | – | 3 ± 0.4 |

Table 4.2 *Tensile properties of copolymer PET and its nanocomposites with hexadecylimidazolium, $im_{16}$, montmorillonite, as processed (extruded and injection-molded) and after annealing at 140 °C for 1.5 h under $N_2$*

| MMT content $\varphi_{mmt}$ (wt%) | Tensile modulus $E$ (MPa) | Yield strength $\sigma_{yield}$ (MPa) | Strengthk at break $\sigma_{max}$ (MPa) | Elongation at break $\varepsilon_{max}$ (%) |
|---|---|---|---|---|
| co-PET/$C_{16}$-imidaz-MMT, as processed | | | | |
| 0 | 1780 | 62 | 31 | 82 |
| 3 $im_{16}$ | 2066 | 60 | 34 | 90 |
| 6 $im_{16}$ | 2308 | 59 | 46 | 5 |
| co-PET/$C_{16}$-imidaz-MMT, annealed | | | | |
| 0 | 2130 | 78 | 37 | 17 |
| 3 $im_{16}$ | 2512 | – | 73 | 4 |
| 6 $im_{16}$ | 2829 | – | 64 | 3 |

for the relatively stiff matrices considered here (unfilled polymer modulus 1.5–2 GPa); however, in most cases, increasing the filler loading resulted in concurrent decrease of the elongation at break, and eventually in dramatic embrittlement of the composite ($\varepsilon_{max} < 10\%$). For example, addition of alkylammonium montmorillonite (2MTL8-MMT) to homo-PET at 3 wt% decreases $\varepsilon_{max}$ from 230% to 115% (Table 4.1), and increasing the filler concentration to 6 wt% further reduces $\varepsilon_{max}$ to 3% (the composite breaks under tensile deformation in a brittle manner, without showing a definitive yield point). Beyond any PET decomposition, this behavior was traced [44] in the changes of the PET crystallization upon addition of alkylammonium montmorillonite, which acts a heterogeneous nucleating agent for homo-PET, nucleating crystallites (spherulites, dendrites, etc.) with sizes comparable

to the filler–filler separation distance [33, 45]; with increasing filler concentration the PET crystallites become increasingly small, unable to accommodate high tensile strains, causing the composite to catastrophically fail at very low strains. The tensile behavior of the PET/alkylammonium MMT systems is very similar to that of PET polymerized in the presence of surfactant-free/$Na^+$-MMT [45], hinting that the alkylammonium may have decomposed markedly during melt-processing. The tensile behavior of the PET/MMT nanocomposites can be improved by modifying the clay nanofillers with thermally stable surfactants; for example, a 3 wt% hexadecylimidazolium montmorillonite only reduces the elongation at break from 230% to 200%, but it is still necessary to keep the nanofiller concentration below the percolation threshold for these fillers (below ca. 4.5 wt% inorganic).

To further explore the embrittlement of PET upon addition of nanofillers, we investigated the tensile properties of the nanocomposites of PET copolymer with hexadecylimidazolium montmorillonite (Table 4.2). This blow-molding grade of co-PET already contains a noncrystallizable comonomer that reduces the PET crystallization. For practical purposes these polymers are considered to be mainly amorphous, and addition of small amounts of organoclay, for example, 3 wt% MMT, only increases the Young's modulus without affecting the yield point or the stress and strain at break ($\sigma_{max}$, $\varepsilon_{max}$). Increasing the organoclay concentration to 6 wt% dramatically reduces the elongation at break to 5%, because of nanofiller percolation. The tensile behavior upon crystallization in these systems can be revealed by annealing the nanocomposites (140 °C for 1.5 h under nitrogen), which allows crystallization to develop, increasing the crystal fraction and thus the Young's modulus and decreasing the $\varepsilon_{max}$ (Table 4.2). As with the homo-PET, these annealed systems show very low $\varepsilon_{max}$ (3–4%) and the absence of a definitive yield point. These results illustrate that in a mostly amorphous PET nanocomposite, the $\varepsilon_{max}$ is also affected for high nanofiller loadings, where a percolated filler network associated with the dispersed silicate layers [46] causes decreased mobilities for the PET chains; whereas, for crystallizable PET nanocomposites, $\varepsilon_{max}$ is dramatically decreased when the crystallite size reduction leads to inability of the crystallites to align properly during deformation, causing brittle failure. Thus, when the composites based on the two different PET matrices are compared, despite the apparent similar tensile behavior ($E$ increases systematically with organoclay addition, and $\varepsilon_{max}$ decreases dramatically beyond the percolation filler concentration) different mechanisms are responsible in each case. However, in both cases, the magnitude of improvement in $E$ suggests that the interfacial adhesion between PET and imidazolium–MMT is sufficiently strong to transfer the external stress to the filler (up to $E \sim$ 2–2.5 GPa), and is stronger than that of alkylammonium MMT; further, to maintain the PET ductility in MMT-based nanocomposites, the organofiller loading needs to be below the percolation filler concentration for both amorphous and crystallizable PET matrices.

Trends similar to those for the tensile properties can be observed in the thermomechanical properties of these nanocomposites. In Figure 4.6 we compare the dynamic mechanical response of a homo-PET with that of its nanocomposites at 3 wt% MMT (melt-processed with alkylammonium, 2MTL8, and alkylimidazolium, $C_{16}$-imidaz, montmorillonites). It is clear that the storage moduli of the nanocomposites are higher than that of the unfilled PET

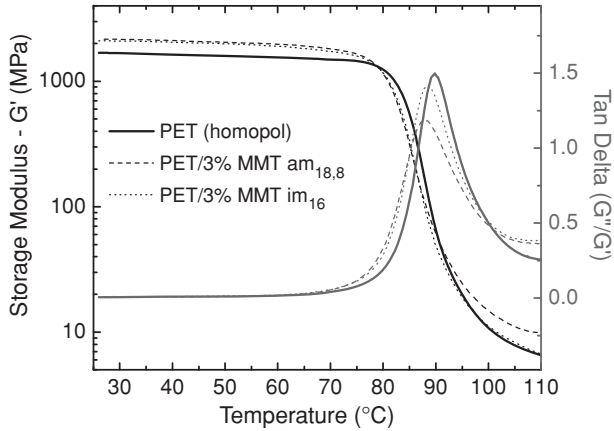


Figure 4.6 DMA analysis comparing unfilled PET homopolymer with melt-processed PET nanocomposites at 3 wt% inorganic loading, based on hexadecylimidazolium MMT ($im_{16}$) and on 2MTL8 alkylammonium MMT ($am_{18,8}$). The storage modulus ($G'$) and the tan$\delta$ ($G''/G'$) are plotted.

matrix (2.10 GPa at 30 °C, compared to 1.67 GPa for unfilled PET). This improvement in modulus persists up to the softening temperature of the matrix, around 80 °C, and is also present – albeit with a smaller relative increase – at high temperatures ($G'$ plateau). Here it is of interest to note the difference in behavior around the softening temperature, for example, as manifested in the tan$\delta$ peak, where the composites based on alkylammonium MMT depart significantly more from the PET matrix response than those with the more thermally stable alkylimidazolium surfactants. This difference reflects the better thermal stability of the PET/alkylimidazolium MMT composites, because thermal decomposition of the PET in the presence of alkylammonium MMT leads to reduced polymer molecular weights, which, in turn, lead to a lowering of the apparent glass transition temperature ($T_g$).

### *4.3.3 Thermal and fire properties*

The TGA results of co-PET and its melt-processed nanocomposites are given in Figure 4.7 (a, b). The addition of alkylimidazolium montmorillonite has no effect on the decomposition temperature at the maximum weight-loss rate ($T_{d\ \max}$) of the co-PET under inert conditions (nitrogen), whereas this organoclay's addition caused an increase of the $T_{d\ \max}$ of the co-PET in the oxidizing environment (air). These results indicate that the nanocomposites exhibit enhanced thermal stability, as would be expected. This behavior is identical for the homo-PET reinforced with the same alkylimidazolium montmorillonite (also melt-processed), as well as for the homo-PET reinforced by alkylammonium montmorillonite (Table 4.3); in this last case, TGA probably records the PET decomposition in the presence of "bare" MMT fillers/layers [45], because most of the alkylammoniums decomposed during the melt-processing. In all cases under air, the second decomposition temperature $T^2_{d\max}$ probably includes contributions from the MMT dehydroxylation – resulting in a broader

Table 4.3 *Summary of TGA*

| Materials | Under nitrogen[a] | | In air[a] | | |
|---|---|---|---|---|---|
| | $T_{d\,\max}$ [b] (°C) | Char[c] (wt%) | $T^1_{d\,\max}$ [b] (°C) | $T^2_{d\,\max}$ [d] (°C) | Char[c] (wt%) |
| Co-PET (unfilled) | 435 | 2.7 | 430 | 549 | 0.5 |
| Co-PET/3wt% $im_{16}$ | 435 | 5.2 | 437 | 560 | 4.8 |
| Co-PET/6wt% $im_{16}$ | 434 | 13.6 | 435 | 562 | 6.2 |
| Homo-PET (unfilled) | | | 439 | 550 | 0.0 |
| Homo-PET/3wt% $im_{16}$ | | | 441 | 569 | 3.1 |
| Homo-PET/3wt% $am_{18,8}$ | | | 438 | 553 | 4.4 |

[a] Gas flow rate 100 mL/mm; heating rate 10 °C/min.
[b] Decomposition temperature at the maximum weight-loss rate.
[c] Amount of the nonvolatile residue measured at the highest temperature (900 °C).
[d] Decomposition temperature at second maximum weight-loss rate.

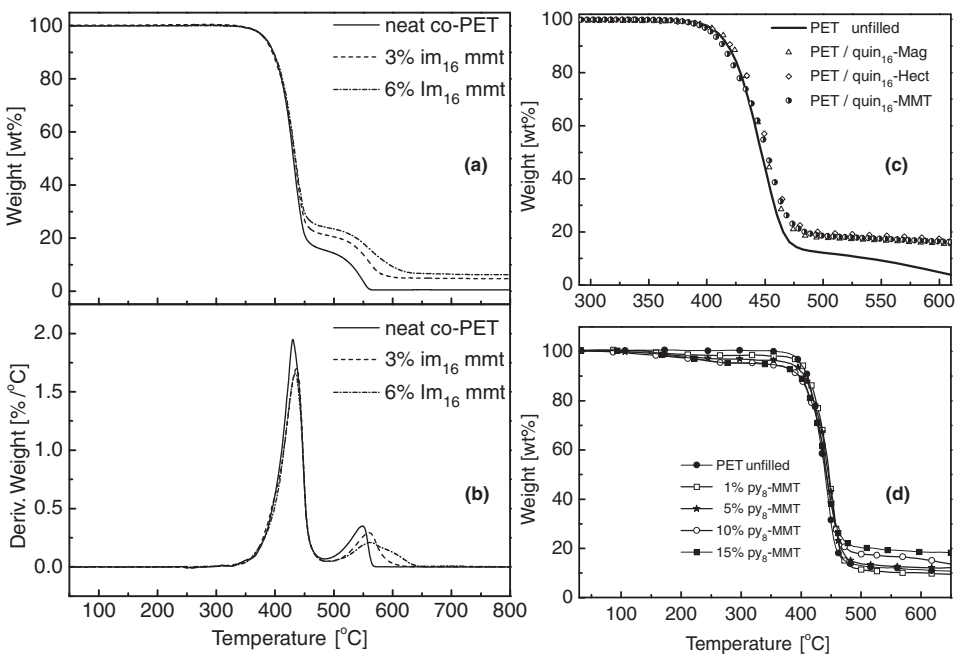


Figure 4.7 Thermogravitometric analysis (TGA) of various PET nanocomposites employing clays with thermally stable organic surfactants: (a,b) Melt-processed PET copolymer with hexadecylimidazolium MMT; (c) Melt-processed PET homopolymer with various clays bearing hexadecylquinoliniums [25]. (d) Solution-processed PET with cetylpyridinium MMT [22]. All TGA was done under $N_2$ flow.

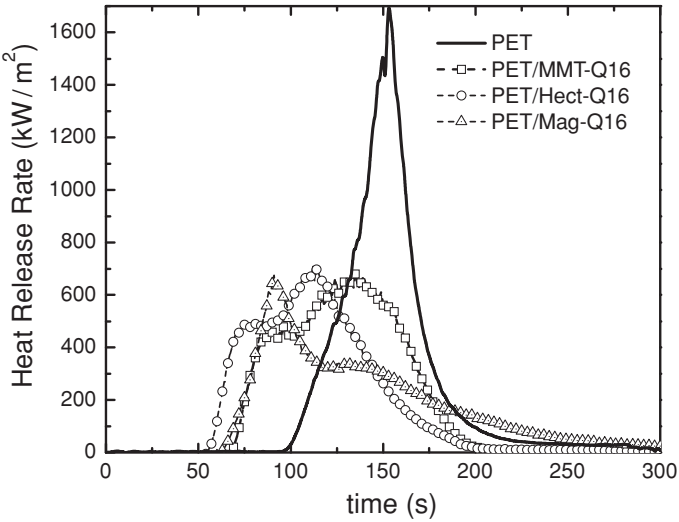


Figure 4.8 Cone calorimetry of homopolymer PET with various clays modified by hexadecylquinolinium (montmorillonite (MMT), hectorite (Hect), and magadiite (Mag)]. Figure adopted with permission from Costache *et al*. [25], © 2006 Wiley.

peak in the differential TGA, Figure 4.7 (b) – and any improvements in $T^2_{d\,\max}$ cannot be definitively attributed to thermal improvements in the nanocomposites. This behavior also strongly resembles that of PET/organoclay melt-processed nanocomposites reinforced with alkylquinolinium MMT [Figure 4.7 (c)], and also of PET/alkylpyridinium-MMT nanocomposites formed by solution mixing [22] [Figure 4.7 (d)]; thus, this TGA response is characteristic of PET in the presence of MMT bearing thermally stable surfactants. It is interesting to note that the addition of imidazolium montmorillonite in co-PET greatly improved the amount of char, from 2.7% in the case of virgin PET to about 14% for the 6 wt% nanocomposite, in close agreement with what was previously observed for homo-PET/alkylquinolinium MMT nanocomposites [25].

Finally, because the TGA showed no deterioration in the PET thermal decomposition, it is of interest to characterize the fire performance of these nanocomposites as well. This was done by cone calorimetry for the alkylquinolinium MMT–reinforced homo-PET [25]. In Figure 4.8 we show the response of PET and its nanocomposites with three clays bearing thermally stable alkylquinolinium surfactants, measured at an incident flux of 35 kW/mm$^2$ on thermally thin (3-mm) specimens. These cone results were typical for polymer/clay nanocomposites, with the total heat release remaining unchanged, similarly to that of the unfilled PET, whereas the peak heat release rate (PHRR) is significantly reduced compared to the respective unfilled PET. At the same time, the mass loss rates are approximately constant for the three montmorillonite nanocomposites, and there is a more prolonged burning time for all the nanocomposites (evidenced by the shape of the HRR curves) accompanied by a decrease in the time-to-ignition (Figure 4.8). This previous

study [25] concluded that this fire performance is probably due to filler-induced increased char formation, because the reductions in PHRR are roughly comparable for all four composites, despite their morphological variations (ranging from very good nanoscale and mesoscale dispersions for the MMT-based nanocomposites to rather poor dispersions and conventional composite structures for the magadiite-based composites [25]). In addition, when the fire behavior of these PET nanocomposites [25] was compared with that of PS nanocomposites [47] (based on both alkylquinolinium- and alkylammonium-modified MMT), it was suggested that the thermally stable quinolinium surfactants are more effective in fire-resistance improvement than the alkylammonium surfactants [25].

## 4.4 Conclusions

Nanoclays with thermally stable surfactant modifications were explored for use in melt-processed PET nanocomposites. Both alkylimidazolium and alkylquinolinium surfactants offer viable alternatives to the common alkylammoniums, and both resulted in well-performing PET nanocomposites. The melt-processing of PET composites with clays bearing these thermally stable surfactants does not require any changes in the standard practices of PET processing. The composite morphology of the melt-processed PET nanocomposites showed good nanofiller dispersion, which, in turn, resulted in good mechanical and thermal properties for the nanocomposites. For optimum mechanical improvement, the filler loading needs to be smaller than the filler percolation threshold concentration, for both amorphous and crystalline PET; for filler concentrations higher than this, marked embrittlement of the PET nanocomposite is observed.

## 4.5 Experimental

### *4.5.1 Synthesis of alkylimidazoles*

As an example of a monoalkylimidazole surfactant, we describe the synthesis of 1-hexadecylimidazolium iodide [Figure 4.1 (a)] based on prior work [26]. An amount of 0.500 g (7.35 mmol) of imidazole was completely dissolved in 50 mL of tetrahydrofuran (THF) in a 100-mL flask with a reflux condenser. Subsequently, 2.590 g (7.35 mmol) of 1-iodohexadecane was added dropwise to the flask while it was stirred at 55–60 °C.

The reactants were heated to reflux with stirring for approximately 12 h. At this point, complete consumption of imidazole can be verified by $^1$H NMR, through the disappearance of the peak at the 11.8-ppm chemical shift (assigned to the proton connected to the imidazole ring nitrogen: cf. Figure 1 in Ref. [26]). The solution was dried by removal of the THF, and a yellow solid was obtained; this solid was washed three times in 20 mL of hexane. The complete removal of unreacted 1-iodohexadecane can be verified by the absence of the $^1$H peak at 3.28 ppm attributed to the $CH_2$ adjacent to the iodine in the 1-iodohexadecane. The resulting solid was fully protonated in 30 mL of 1 wt% hydrochloric acid solution in methanol for 1 h, and subsequently dried under vacuum to get a yellow solid, yielding 2.3 g

of product (74% yield). To obtain a dialkylimidazole [Figure 4.1 (b)], a similar synthesis can be carried out, using a higher reaction temperature and an excess of 1-iodohexadecane [26]. An amount of 0.500 g (7.35 mmol) of imidazole was dissolved in 50 mL of THF and 7.770 g (three times the moles of imidazole) of 1-iodohexadecane was added dropwise to the flask while it was stirred. The solution was heated to reflux for approximately 48 h at 60–75 °C. After the removal of THF, the resulting purple-yellow solid was washed with large quantities of pentane to remove the unreacted 1-iodohexadecane, protonated with 1 wt% hydrochloric acid solution in methanol for 1 h, and subsequently dried under vacuum to yield 2.8 g of product (34% yield).

### *4.5.2 Synthesis of alkylquinoline*

Hexadecylquinolinium [Figure 4.1 (c)] was prepared by the reaction of quinoline with 1-bromohexadecane. In a 250-mL flask, 10.0 g (77.4 mmol) of quinoline was dissolved in 150 mL of acetone by stirring for a few minutes. To this solution, 23.6 g (77.4 mmol) of bromohexadecane was added gradually, and then the mixture was refluxed for 48 h. Most of the solvent was removed under vacuum, followed by cooling to room temperature, upon which crystallization occurred. The sample was then washed with ether and filtered (5% yield).

### *4.5.3 Preparation of organically modified montmorillonites*

For all cationic surfactants, the preparation of the organically modified nanoclays is carried out via a common cation exchange reaction with $Na^+$ montmorillonite. For example, in the case of alkylimidazolium [26], a large excess of the surfactant (twice the CEC of montmorillonite), was dissolved in ethanol at 50 °C and was added to a 1 wt% aqueous suspension of the montmorillonite under vigorous stirring. The mixture was stirred for 8 h at 50 °C, before the imidazolium-exchanged silicates were collected by filtration. The solids were subsequently washed with hot ethanol and paper-filtered 3–4 times, until an $AgNO_3$ test indicated the absence of halide anions. The filtrate was dried at room temperature, ground, and further dried at 80 °C under vacuum for 24 h, before being hermetically stored in a desiccator at nearly 0% RH.

### *4.5.4 Preparation of PET nanocomposites*

Nanocomposites were prepared by melt-blending PET polymer with organically modified MMT. A variety of processing equipment was used, typically operated at 280 °C: a Brabender plasticorder twin-head kneader (7 min at 280 °C and 60 rpm) for PET/quinolinium–MMT, a Prism TSE 16TC extruder with an L/D ratio of 16 (280 °C at a screw speed of 280–330 rpm) for large-scale PET/imidazolium–MMT (10–30 lb/h), and a laboratory-scale Haake counter-rotating twin screw extruder with an L/D ratio of 20 (280 °C at a screw speed

of 50 rpm) for smaller-scale PET/imidazolium–MMT (5 lb/h). Prior to extrusion, all materials were dried overnight under vacuum at 100 °C and were tumbled-mixed for 20 min. Subsequent preparation of tensile dogbone specimens was done in a Boy 22D 24-ton injection molding machine (operated at 295 °C, with the mold at ambient temperature).

### *4.5.5 Mechanical characterization*

The mechanical properties of the bulk PET and its nanocomposites were measured by tensile testing on injection-molded tensile bars (dogbones) and by DMA on injection-molded bars. The dogbones are ASTM D638 type IV specimens with a molded thickness of approximately 3.18 mm. An Instron 5866 tensile tester was operated with a cross-head speed of 50.8 mm/min. The Young's modulus, yield strength, and elongation at break are reported per the calculations from stress–strain curves done with the Instron software. The elongation at break is reported from the cross-head travel, as a strain extensometer with sufficient travel was unavailable. It is also important to note that the tensile behavior was typically measured on the as-molded tensile bars with no postmolding annealing, unless otherwise noted. DMA was also utilized to examine the thermomechanical behavior on a TA Instruments Q800 instrument with a 35-mm dual-cantilever setup. Such tests probe the response of the material to oscillatory deformation (1 Hz, at a constant strain of 0.01%, ramping temperature from 25 to 170 °C at a rate of 4 °C/min) and determine the storage ($G'$) and loss ($G''$) modulus, and through $\tan\delta = G''/G'$ the material's character for energy dissipation (the temperature of the $\tan\delta$ peak is also a good indicator of the apparent glass transition temperature, $T_g$).

## References


1. T. J. Pinnavaia and G. W. Beall, eds., *Polymer–Clay Nanocomposites* (West Sussex, UK: Wiley, 2000).
2. L. Utracki, *Clay-Containing Polymeric Nanocomposites* (Shropshire, UK: Rapra Tech, 2004).
3. Y. Mai and Z. Yu, eds., *Polymer Nanocomposites* (Cambridge, UK: Woodhead, 2006).
4. A. B. Morgan and C. A. Wilkie, eds., *Polymer Nanocomposite Flammability* (Hoboken, NJ: Wiley, 2006).
5. E. Manias, Nanocomposites – Stiffer by design. *Nature Materials*, 6 (2007), 9–11.
6. B. K. G. Theng, *Formation and Properties of Clay–Polymer Complexes* (Amsterdam: Elsevier, 1979).
7. B. K. G. Theng, *Chemistry of Clay–Organic Reactions* (New York: Wiley, 1974).
8. Y. Kojima, A. Usuki, M. Kawasumi, A. Okada, Y. Fukushima, T. T. Kurauchi, and O. Kamigaito, Synthesis and mechanical properties of nylon-6/clay hybrid. *Journal of Materials Research*, 8 (1993), 1179–84 and 1185–9.
9. Y. Kojima, A. Usuki, M. Kawasumi, A. Okada, T. T. Kurauchi, and O. Kamigaito, Synthesis of nylon-6/clay hybrid by montmorillonite intercalated with ε-caprolactam. *Journal of Polymer Science, Part A: Polymer Chemistry*, 31 (1993), 983–6.

10. R. A. Vaia, H. Ishii, and E. P. Giannelis, Synthesis and properties of 2-dimensional nanostructures by direct intercalation of polymer melts in layered silicates. *Chemistry of Materials*, 5 (1993), 1694–6.
11. J. Gilman, C. Jackson, A. Morgan, R. Harris, E. Manias, E. Giannelis, M. Wuthenow, D. Hilton, and S. Phillips, Flammability properties of polymer/layered-silicate nanocomposites: Polypropylene and polystyrene nanocomposites. *Chemistry of Materials*, 12 (2000), 1866–73.
12. P. C. LeBaron, Z. Wang, and T. J. Pinnavaia, Polymer-layered silicate nanocomposites: An overview. *Applied Clay Science*, 15 (1999), 11–29.
13. E. P. Giannelis, R. Krishnamoorti, and E. Manias, Polymer-silicate nanocomposites: Model systems for confined polymers and polymer brushes. *Advances in Polymer Science*, 138 (1999), 107–47.
14. M. Alexandre and P. Dubois, Polymer-layered silicate nanocomposites: Preparation, properties and uses of a new class of materials. *Materials Science and Engineering R: Reports*, 28 (2000), 1–63.
15. S. S. Ray and M. Okamoto, Polymer/596 layered silicate nanocomposites: A review from preparation to processing. *Progress in Polymer Science*, 28 (2003), 1539–1641.
16. E. Manias, A. Touny, L. Wu, K. Strawhecker, B. Lu, and T. C. Chung, Polypropylene/montmorillonite nanocomposites. Review of the synthetic routes and materials properties. *Chemistry of Materials*, 13 (2001), 3516–23.
17. R. A. Vaia and E. P. Giannelis, Lattice model of polymer melt intercalation in organically-modified layered silicates. *Macromolecules*, 30 (1997), 7990–99.
18. R. A. Vaia and E. P. Giannelis, Polymer melt intercalation in organically modified layered silicates: Model predictions and experiment. *Macromolecules*, 30 (1997), 8000–8009.
19. A. C. Balazs, C. Singh, and E. Zhulina, Modeling the interactions between polymers and clay surfaces through self-consistent field theory. *Macromolecules*, 31 (1998), 8370–81.
20. F. Leroux and J. Besse, Polymer interleaved layered double hydroxide: A new emerging class of nanocomposites. *Chemistry of Materials*, 13 (2001), 3507–15.
21. X. L. Xie, Y.-W. Mai, and X. P. Zhou, Dispersion and alignment of carbon nanotubes in polymer matrix: A review. *Materials Science and Engineering R: Reports*, 49 (2005), 89–112.
22. C. Ou, M. Ho, and J. Lin, Synthesis and characterization of poly(ethylene terephthalate) nanocomposites with organoclay. *Journal of Applied Polymer Science*, 91 (2004), 140–45.
23. J. Chang, S. Kim, Y. Joo, and S. Im, Poly(ethylene terephthalate) nanocomposites by in situ interlayer polymerization: The thermo-mechanical properties and morphology of the hybrid fibers. *Polymer*, 45 (2004), 919–26.
24. C. H. Davis, L. J. Mathias, J. W. Gilman, D. A. Schiraldi, J. R. Shields, P. C. Trulove, T. E. Sutto, and H. C. de Long, Effects of melt-processing conditions on the quality of poly(ethylene terephthalate) montmorillonite clay nanocomposites. *Journal of Polymer Science, Part B: Polymer Physics*, 40 (2002), 2661–6.
25. M. C. Costache, M. J. Heidecker, E. Manias, and C. A. Wilkie, Preparation and characterization of poly(ethylene terephthalate)/clay nanocomposites by melt blending using thermally stable surfactants. *Polymers for Advanced Technologies*, 17 (2006), 764–71.

26. Z. M. Wang, T. C. Chung, J. W. Gilman, and E. Manias, Melt-processable syndiotactic polystyrene/montmorillonite nanocomposites. *Journal of Polymer Science, Part B: Polymer Physics*, 41 (2003), 3173–87.
27. R. C. MacKenzie, ed., *The Differential Thermal Investigation of Clays* (London: Mineralogical Society, 1957).
28. C. J. van Oss, M. K. Chaudhury, and R. J. Good, Interfacial Lifschitz–van der Waals and polar interactions in macroscopic systems. *Chemical Reviews*, 88 (1988), 927–41.
29. C. J. van Oss, *Interfacial Forces in Aqueous Media* (New York: Dekker, 1994).
30. W. Wu, R. F. Giese, and C. J. van Oss, Evaluation of the Lifshitz–van der Waals/acid–base approach to determine surface tension components. *Langmuir*, 11 (1995), 379–82.
31. D. M. Fox, W. H. Awad, J. W. Gilman, P. H. Maupin, H. C. de Long, and P. C. Trulove, Flammability, thermal stability, and phase change characteristics of several trialkylimidazolium salts. *Green Chemistry*, 5 (2003), 724–7.
32. J. W. Gilman, W. H. Awad, R. D. Davis, J. Shields, R. H. H. Jr., C. Davis, A. B. Morgan, T. E. Sutto, J. Callahan, P. C. Trulove, and H. C. DeLong, Polymer/layered-silicate nanocomposites from thermally stable trialkylimidazolium-treated montmorillonite. *Chemistry of Materials*, 14 (2002), 3776–85.
33. S. Monemian, V. Goodarzi, P. Zahedi, and M. Angaji, PET/imidazolium based OMMT nanocomposites via in situ polymerization: Morphological, thermal, and nonisothermal crystallization studies. *Advances in Polymer Technology*, 26 (2007), 247–57.
34. A. Vassiliou, K. Chrissafis, and D. Bikiaris, Thermal degradation kinetics of in situ prepared PET nanocomposites with acid-treated multi-walled carbon nanotubes. *Journal of Thermal Analysis and Calorimetry*, 100 (2010), 1063–71.
35. J. Langat, S. Bellayer, P. Hudrlik, A. Hudrlik, P. H. Maupin, J. W. Gilman, Sr., and D. Raghavan, Synthesis of imidazolium salts and their application in epoxy montmorillonite nanocomposites. *Polymer*, 47 (2006), 6698–709.
36. M. Modesti, S. Besco, A. Lorenzetti, M. Zammarano, V. Causin, C. Marega, J. W. Gilman, D. M. Fox, P. C. Trulove, H. C. de Long, and P. H. Maupin, Imidazolium-modified clay-based ABS nanocomposites: A comparison between melt-blending and solution-sonication processes. *Polymers for Advanced Technologies*, 19 (2008), 1576–83.
37. M. Modesti, S. Besco, A. Lorenzetti, V. Causin, C. Marega, J. W. Gilman, D. M. Fox, P. C. Trulove, H. C. De Long, and M. Zammarano, ABS/clay nanocomposites obtained by a solution technique: Influence of clay organic modifiers. *Polymer Degradation and Stability*, 92 (2007), 2206–13.
38. D. M. Fox, P. H. Maupin, R. H. Harris, Jr., J. W. Gilman, D. V. Eldred, D. Katsoulis, P. C. Trulove, and H. C. De Long, Use of a polyhedral oligomeric silsesquioxane (POSS)–imidazolium cation as an organic modifier for montmorillonite. *Langmuir*, 23 (2007), 7707–14.
39. S. Bellayer, J. Gilman, N. Eidelman, S. Bourbigot, X. Flambard, D. Fox, H. De Long, and P. Trulove, Preparation of homogeneously dispersed multiwalled carbon nanotube/polystyrene nanocomposites via melt extrusion using trialkyl imidazolium compatibilizer. *Advanced Functional Materials*, 15 (2005), 910–16.
40. R. A. Vaia and W. D. Liu, X-ray powder diffraction of polymer/layered silicate nanocomposites: Model and practice. *Journal of Polymer Science, Part B: Polymer Physics*, 40 (2002), 1590–1600.
41. R. A. Vaia, W. D. Liu, and H. Koerner, Analysis of small-angle scattering of suspensions of organically modified montmorillonite: Implications to phase behavior of polymer

nanocomposites. *Journal of Polymer Science, Part B: Polymer Physics*, 41 (2003), 3214–36.
42. H. J. M. Hanley, C. D. Muzny, D. L. Ho, C. J. Glinka, and E. Manias, A SANS study of organoclay dispersions. *International Journal of Thermophysics*, 22 (2001), 1435–48.
43. A. Morgan and J. Gilman, Characterization of polymer-layered silicate (clay) nanocomposites by transmission electron microscopy and X-ray diffraction: A comparative study. *Journal of Applied Polymer Science*, 87 (2003), 1329–38.
44. M. J. Heidecker, H. Nakajima, and E. Manias, Structure and properties of PET/montmorillonite nanocomposites prepared by melt-blending. *Polymers for Advanced Technologies* (in press).
45. Z. Chen, P. Luo, and Q. Fu, Preparation and properties of organo-modifier free PET/MMT nanocomposites via monomer intercalation and in situ polymerization. *Polymers for Advanced Technologies*, 20 (2009), 916–25.
46. L. Xu, H. Nakajima, E. Manias, and R. Krishnamoorti, Tailored nanocomposites of polypropylene with layered silicates. *Macromolecules*, 42 (2009), 3795–803.
47. G. Chigwada, D. Wang, and C. Wilkie, Polystyrene nanocomposites based on quinolinium and pyridinium surfactants. *Polymer Degradation and Stability*, 91 (2006), 848–55.